

# Improving the linear flexibility distribution model to simultaneously account for gravity and lateral loads

AliReza Habibi\*<sup>1</sup> and Mehdi Izadpanah<sup>2a</sup>

<sup>1</sup>Department of Civil Engineering, Shahed University, Tehran, Iran  
<sup>2</sup>Department of Civil Engineering, University of Kurdistan, Sanandaj, Iran

(Received November 22, 2016, Revised February 5, 2017, Accepted February 12, 2017)

**Abstract.** There are two methods to model the plastification of members comprising lumped and distributed plasticity. When a reinforced concrete member experiences inelastic deformations, cracks tend to spread from the joint interface resulting in a curvature distribution; therefore, the lumped plasticity methods assuming plasticity is concentrated at a zero-length plastic hinge section at the ends of the elements, cannot model the actual behavior of reinforced concrete members. Some spread plasticity models including uniform, linear and recently power have been developed to take extended inelastic zone into account. In the aforementioned models, the extended inelastic zones in proximity of critical sections assumed close to connections are considered. Although the mentioned assumption is proper for the buildings simply imposed lateral loads, it is not appropriate for the gravity load effects. The gravity load effects can influence the inelastic zones in structural elements; therefore, the plasticity models presenting the flexibility distribution along the member merely based on lateral loads apart from the gravity load effects can bring about incorrect stiffness matrix for structure. In this study, the linear flexibility distribution model is improved to account for the distributed plasticity of members subjected to both gravity and lateral load effects. To do so, a new model in which, each member is taken as one structural element into account is proposed. Some numerical examples from previous studies are assessed and outcomes confirm the accuracy of proposed model. Also comparing the results of the proposed model with other spread plasticity models illustrates glaring error produced due to neglecting the gravity load effects.

**Keywords:** distributed plasticity; reinforced concrete; inelastic deformations; linear flexibility distribution; gravity load

## 1. Introduction

Recognition of the actual inelastic behavior of structures is necessary to design new ones or to rehabilitate existing structures. When a structure is subjected to severe earthquake, deforming well and dissipating the imposed energy is expected. To model the nonlinear analysis of reinforced concrete structures, many analytical models have been introduced. These analytical models include very refined and complex local models and simplified global models. In refined models, the structural behavior of elements is considered in detail; therefore, small structures or structural subassemblies are typically analyzed using these models. Contrary to refined models, simplified global models have been typically used for analysis of large structures. Although refined models consider more properties of structures in analysis, their time-consuming and calculus complexity make the cost of analysis very high, so these models are not proper to nonlinear analysis of reinforced concrete frames. On the other hand, global models are not appropriate to model the actual behavior of critical region of structures. In fact, the global models use the outcomes of local models obtained for critical regions

and the local models require the results of global models for loading history; therefore, the accuracy of the consequences of refined models for critical region of structures completely depends on global models and vice versa.

Since the aim of this study is the nonlinear analysis of reinforced concrete frames, the global models are taken into account. To simulate the plastification of structures simply and efficiently, some macro-models (global) have been presented to date. These models are usually traced the change of structural properties like stiffness and strength along the members and are divided into two categories. The first category is the lumped plasticity (concentrated plastic hinge) and the second one is the distributed plasticity approach (spread plasticity). In the lumped plasticity models, it is assumed that plastification is concentrated in the two ends of element and the member between two zero-length hinges remains fully elastic. Although this method is a computationally simple and efficient way to take the effect of inelastic material, it over predicts the limit strength of structures that can bring about unsafe designs (King *et al.* 1992, White 1993, McGuire 1994). The research of Clough (1966), Giberson (1967), Al-Haddad and Wight (1968) and Aoyama and Sugano (1968) are from the first studies in this category. Otani and Sozen (1972) put forward “connected two-cantilever model”. As an option for concentrated plasticity, Kunnath and Reinhorn (1989) proposed a concentrated plasticity model used in IDARC2D (Park *et al.* 1987). To evaluate the effect of different hysteretic models, Anderson and Townsend (1977) considered four different

\*Corresponding author, Associate Professor

E-mail: [ar.habibi@uok.ac.ir](mailto:ar.habibi@uok.ac.ir)

<sup>a</sup>Ph.D. Student

types of hysteretic models. They concluded that the trilinear degrading connection model has the highest accuracy among the assessed hysteretic models. Inel and Ozmen (2006) studied the effect of plastic hinge properties in nonlinear analysis of reinforced concrete buildings. Alva and de Cresce El Debs (2010) applied a lumped dissipation model to nonlinear analysis of reinforced concrete structures. Birely *et al.* (2012) presented a model to simulate the nonlinear response of planar reinforced-concrete frames including all sources of flexibility. They modeled nonlinearity introducing a dual-hinge lumped-plasticity beam element comprising of two rotational springs in series; one spring simulates beam flexural response and another one models joint response. Zhao *et al.* (2012) evaluated the plastic hinge length in reinforced concrete flexural members. They analytically considered the performance of the plastic hinge zone with Finite Element Method.

In the distributed plasticity models, flexibility is considered based on prescribed distribution pattern of flexural flexibility along the length of member. The parabolic-inflexion distribution (Takizawa 1973) and linear-inflexion distribution (Park *et al.* 1987) fall into this category. In parabolic-inflexion model, an elastic flexibility is taken at the inflection point into account. The linear-inflexion proposed by Park *et al.* (1987) was introduced in the original version of IDARC2D developed by Reinhorn *et al.* (2009). Depending on the location of inflection point is one of shortcomings in the parabolic-inflexion and the linear-inflexion models. To obviate this defect, two spread plasticity models that are linear and uniform flexibility distribution were proposed. In these two models, the flexibility varies only in inelastic zones while the rest of the member is elastic with constant flexibility (Kunnath and Reinhorn 1989). It is worth noting that in the plasticity models, the fiber model approach is utilized to acquire the moment-curvature relationship of the end sections (Mander 1984). The fiber model can consider any hardening and softening stress-strain behavior (Roh *et al.* 2012). Kim and Kurama (2008) used the spread plasticity model to capture flexural nonlinearity. Roh *et al.* (2012) introduced a power spread plasticity model to inelastic analysis of reinforced concrete. They demonstrated that the high order spread plasticity models produce smaller displacement and higher acceleration, in the structural system. Hajjar *et al.* (1998) presented the constitutive formulation and cyclic analysis capability of a three-dimensional fiber-based distributed plasticity finite element for square or rectangular concrete-filled steel tube (CFT) beam-columns. Lee and Filippou (2009) proposed a new flexibility-based finite element model with a variable inelastic zone model. Nguyen and Kim (2014) put forward a displacement-based finite element procedure to analyze of plane steel frames with nonlinear beam-to-column connections. IU (2016) used a method of the refined plastic hinge approach to nonlinear analysis of reinforced concrete structures.

As pointed out, when reinforced concrete members encounter inelastic deformation, cracks tend to spread along the length of members; therefore, spread plasticity models are more proper than lumped plasticity for these members. In most of spread plasticity models like the linear flexibility

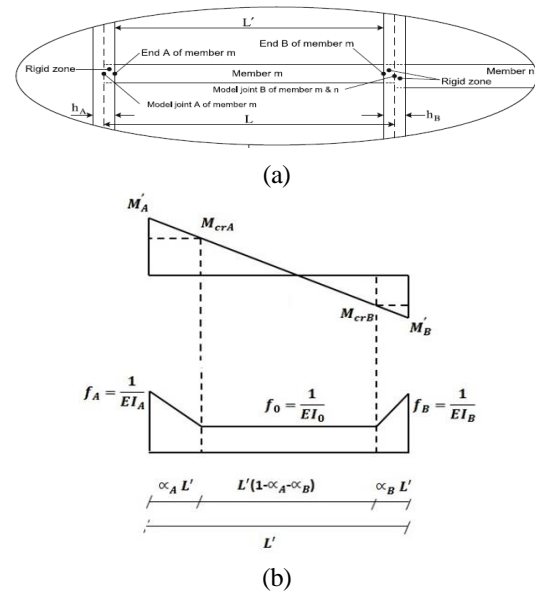


Fig. 1(a) Rigid zone and ends definitions of a RC element (b) moment distribution and linear flexibility distribution (Reinhorn *et al.* 2009)

that is one of prevalent models for reinforced concrete elements; prescribed distribution pattern of flexural flexibility is merely based on the lateral load effect. Neglecting gravity load effect, especially in cases of significant gravity load moments can induce a glaring error as it was illustrated by Izadpanah and Habibi (2015). They pointed out that in incremental nonlinear analyses; disregarding the gravity load effects can lead to incorrect results, because the tangent stiffness matrix at each load step depends on plasticity models in all previous steps and gravity load effects in many of these prior steps dominate the lateral loads. In the other words, ignoring gravity load effect in plasticity models, not only causes some errors in the tangent stiffness matrix at each step but also produces cumulative errors in the next steps (Izadpanah and Habibi 2015). The main objective of this study is to improve the linear flexibility distribution model for taking both gravity and lateral load effects into account without subdividing the elements. To do so, a new formulation is presented using the unit load theory based on the principle of virtual work. In the proposed model, each member is taken as one element into account; therefore, there is an one-to-one correspondence between structural members (beams and columns) and model elements.

## 2. Section spread plasticity model

### 2.1 The linear flexibility formulation

When an element experiences inelastic deformation, depending on the order of inelasticity, sections along the element display different flexibility values. In the spread plasticity models, the prescribed pattern is taken for explaining the flexibility variation. The Linear Flexibility Model (LFM) is indicated in Fig. 1.

In Fig. 1,  $EI_A$  and  $EI_B$  are the current flexural stiffness of

the sections at ends “A” and “B”, respectively;  $EI_0$  is the equivalent constant stiffness in the elastic portion of the element;  $\alpha_A$  and  $\alpha_B$  are the yield penetration coefficients (Reinhorn *et al.* 2009). The flexural stiffness  $EI_A$  and  $EI_B$  are determined from the hysteretic models. The rotation at each ends can be obtained using the flexural and shear flexibilities as follows

$$\begin{bmatrix} \theta'_A \\ \theta'_B \end{bmatrix} = \begin{bmatrix} f_{AA} & f_{AB} \\ f_{BA} & f_{BB} \end{bmatrix} \begin{bmatrix} M'_A \\ M'_B \end{bmatrix} \quad (1)$$

where  $f_{AA}$ ,  $f_{AB}$  and  $f_{BB}$  are the flexibility coefficients,  $\theta'_A$  and  $\theta'_B$  are the rotations at the ends of the element, while  $M'_A$  and  $M'_B$  are the corresponding moments. The flexibility coefficients in Eq. (1) are extracted using the unit load theory based on the principle of virtual work

$$f_{ij} = \int_0^{L'} \frac{m_i(x)m_j(x)}{EI(x)} dx + \int_0^{L'} \frac{v_i(x)v_j(x)}{GA(x)} dx \quad (2)$$

where  $m_i(x)$  and  $m_j(x)$  are the moment distributions due to a virtual unit moment at ends “i” and “j”, respectively;  $v_i(x)$  and  $v_j(x)$  are the corresponding shear distributions ( $1/L'$ ) (that “i” and “j” can be replaced by “A” or “B” for the element depicted in Fig. 1.);  $EI(x)$  and  $GA(x)$  are flexural and shear stiffness along the element, respectively. The linear flexibility coefficients for the linear flexibility assumption shown in Fig. 1(b) are obtained as follows.

$$f_{AA} = \frac{L'}{12} \left[ \frac{4}{EI_0} + \left( \frac{1}{EI_A} - \frac{1}{EI_0} \right) (6\alpha_A - 4\alpha_A^2 + \alpha_A^3) + \left( \frac{1}{EI_B} - \frac{1}{EI_0} \right) (\alpha_B^3) \right] + \frac{1}{GA_0L'} \quad (3)$$

$$f_{AB} = f_{BA} = \frac{L'}{12} \left[ \frac{-2}{EI_0} - \left( \frac{1}{EI_A} - \frac{1}{EI_0} \right) (2\alpha_A^2 - \alpha_A^3) - \left( \frac{1}{EI_B} - \frac{1}{EI_0} \right) (2\alpha_B^2 - \alpha_B^3) \right] + \frac{1}{GA_0L'} \quad (4)$$

$$f_{BB} = \frac{L'}{12} \left[ \frac{4}{EI_0} + \left( \frac{1}{EI_B} - \frac{1}{EI_0} \right) (6\alpha_B - 4\alpha_B^2 + \alpha_B^3) + \left( \frac{1}{EI_A} - \frac{1}{EI_0} \right) (\alpha_A^3) \right] + \frac{1}{GA_0L'} \quad (5)$$

The above formulation was rewritten and the close-form solutions of the Eqs. (3)-(5) are defined as presented in Reinhorn *et al.* (2009).

The yield penetration coefficients ( $\alpha_A$  and  $\alpha_B$ ) assign the portion of element where the acting moment is greater than the section cracking moment ( $M_{crA}$  or  $M_{crB}$ ).

$$\alpha_A = \frac{M'_A - M_{crA}}{M'_A - M'_B} \quad \text{for} \quad |M'_A| > |M_{crA}| \quad (6)$$

$$\alpha_B = \frac{M'_B - M_{crB}}{M'_B - M'_A} \quad \text{for} \quad |M'_B| > |M_{crB}| \quad (7)$$

These parameters are calculated for the current moment distribution, and then checked with the previous maximum penetration lengths  $\alpha_{Amax}$  and  $\alpha_{Bmax}$ . The yield penetration parameters cannot be smaller than the previous maximum values regardless of the current moment distribution (Reinhorn *et al.* 2009).

As it is clear in Fig. 1, the prescribed linear flexibility pattern was developed based on linear moment distribution.

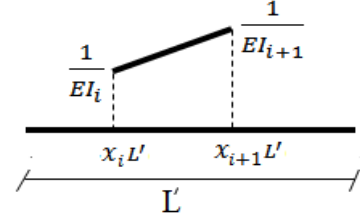


Fig. 2 The assumed linear flexibility between two successive transformation points



Fig. 3 The considered degrees of freedom

Linear moment distribution is proper for members simply subjected lateral loads. Although in IDARC2D report (Reinhorn *et al.* 2009) has been noted that the presence of gravity loads will alter the distribution and in cases of significant gravity load moments the structural elements should be subdivided to capture this variation, subdividing each member to some elements causes big stiffness matrix for each member and the huge stiffness matrix for global structure increasing the time of analysis. Furthermore, the number of parts required was not specified in IDARC2D (Reinhorn *et al.* 2009) so choosing the sufficient one is a trial and error process. Another drawback of the linear flexibility model is that the yielded and cracked lengths are not separated in yield penetration formulation. This obstacle can make errors in the stiffness matrices (Izadpanah and Habibi 2015).

## 2.2 Improving the linear flexibility model

As pointed out, the linear flexibility model has some defects; therefore, in this section an Improved Linear Flexibility Model (ILFM) is put forward to obviate aforementioned shortcomings. To derive new formulation, the flexibility and stiffness coefficients are determined using the unit load theory. The required process to determine the transformation points and the flexibility of each part will be illustrated in the next sections.

### 2.2.1 The proposed model

To develop the ILFM, a general formulation is derived for a member subdivided by “m” transformation points (including both of ends) and the flexibility of each subdivided part is assumed linear (Fig. 2).

In Fig. 2,  $x_i L'$  and  $x_{i+1} L'$  are the positions of two successive transformation points “i” and “i+1” and  $x_i$  and  $x_{i+1}$  are two transformation points coefficients that are the ratios of distance of the points from the left end node to the length. The considered degrees of freedom for the member are according to Fig. 3.

In Fig. 3,  $M_i$ ,  $V_i$  and  $N_i$  are the moment, shear and axial forces of end ‘i’ and  $\theta_i$ ,  $v_i$  and  $u_i$  are the rotation and deformations of it. The parameters of end ‘j’ are similar to end ‘i’.

The flexibility coefficients of the member are determined using the unit load theory based on the principle of virtual work as follows.

$$f_{AA} = \frac{L'}{12} \left( \sum_{i=1}^{m-1} \left( \left( \frac{1}{EI_{i+1}} - \frac{1}{EI_i} \right) (3x_{i+1}^3 - x_{i+1}x_i^2 - x_i x_{i+1}^2 - x_i^3 - 6x_i + 6x_{i+1} - 8x_{i+1}^2 - 8x_{i+1}x_i - 8x_i^2) + \frac{1}{EI_i} (x_{i+1} - x_i)(4x_{i+1}^2 + x_{i+1}x_i + x_i^2 + 12 - 12x_i - 12x_{i+1}) \right) \right) + \frac{1}{L'GA_0} \quad (8)$$

$$-f_{AB} = -f_{BA} = \frac{L'}{12} \left( \sum_{i=1}^{m-1} \left( \left( \frac{1}{EI_{i+1}} - \frac{1}{EI_i} \right) (4x_{i+1}^2 - 2x_{i+1}x_i - 2x_i^2 - 3x_{i+1}^3 + x_{i+1}x_i^2 + 5x_i x_{i+1}^2 - 3x_i^3) + \frac{1}{EI_i} (6x_{i+1}^2 - 6x_i^2 - 4x_{i+1}^3 + 4x_i^3) \right) \right) - \frac{1}{L'GA_0} \quad (9)$$

$$f_{BB} = \frac{L'}{12} \left( \sum_{i=1}^{m-1} \left( \left( \frac{1}{EI_{i+1}} - \frac{1}{EI_i} \right) (3x_{i+1}^3 - x_{i+1}x_i^2 - x_i x_{i+1}^2 - x_i^3) + \frac{4}{EI_i} (x_{i+1} - x_i)(x_{i+1}^2 + x_{i+1}x_i + x_i^2) \right) \right) + \frac{1}{L'GA_0} \quad (10)$$

The above formulation can be rewritten as follows

$$f_{AA} = \frac{L'}{12 \prod_{i=1}^m EI_i} f'_{AA} + \frac{1}{L'GA_0} \quad (11)$$

$$-f_{AB} = -f_{BA} = \frac{L'}{12 \prod_{i=1}^m EI_i} f'_{AB} - \frac{1}{L'GA_0} \quad (12)$$

$$f_{BB} = \frac{L'}{12 \prod_{i=1}^m EI_i} f'_{BB} + \frac{1}{L'GA_0} \quad (13)$$

where

$$f'_{AA} = \sum_{j=1}^{m-1} \left( \left( \prod_{\substack{i=1 \\ i \neq j+1}}^m EI_i - \prod_{\substack{i=1 \\ i \neq j}}^m EI_i \right) (3x_{j+1}^3 - x_{j+1}x_j^2 - x_j x_{j+1}^2 - x_j^3 - 6x_j + 6x_{j+1} - 8x_{j+1}^2 - 8x_{j+1}x_j - 8x_j^2) + \prod_{\substack{i=1 \\ i \neq j}}^m EI_i (x_{j+1} - x_j)(4x_{j+1}^2 + x_{j+1}x_j + x_j^2 + 12 - 12x_j - 12x_{j+1}) \right) \quad (14)$$

$$f'_{AB} = \sum_{j=1}^{m-1} \left( \left( \prod_{\substack{i=1 \\ i \neq j+1}}^m EI_i - \prod_{\substack{i=1 \\ i \neq j}}^m EI_i \right) (4x_{i+1}^2 - 2x_{i+1}x_i - 2x_i^2 - 3x_{i+1}^3 + x_{i+1}x_i^2 + 5x_i x_{i+1}^2 - 3x_i^3) + \prod_{\substack{i=1 \\ i \neq j}}^m EI_i (x_{i+1} - x_i)(6x_{i+1}^2 - 6x_i^2 - 4x_{i+1}^3 + 4x_i^3) \right) \quad (15)$$

$$f'_{BB} = \sum_{j=1}^{m-1} \left( \left( \prod_{\substack{i=1 \\ i \neq j+1}}^m EI_i - \prod_{\substack{i=1 \\ i \neq j}}^m EI_i \right) (3x_{j+1}^3 - x_{j+1}x_j^2 - x_j x_{j+1}^2 - x_j^3) + \prod_{\substack{i=1 \\ i \neq j}}^m 4EI_i (x_{j+1} - x_j)(x_{j+1}^2 + x_{j+1}x_j + x_j^2) \right) \quad (16)$$

In Eqs. (8) to (16),  $EI_i$  is the  $i^{\text{th}}$  stiffness component of the collection "S" and  $x_i$  is  $i^{\text{th}}$  component of the collection "X". Collections "X" and "S" will be explained more

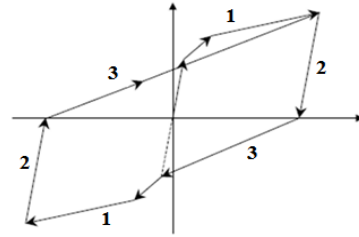


Fig. 4 The vertex oriented hysteric model

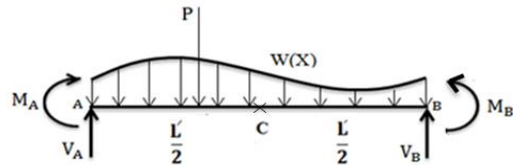


Fig. 5 The element and three considered points

in section 2.2.2. The inverse of the flexibility matrix given by Eq. (1) is the stiffness matrix relating moments and rotations at the ends of the element. Such relation is shown below

$$\begin{bmatrix} M'_A \\ M'_B \end{bmatrix} = \begin{bmatrix} K_{AA} & K_{AB} \\ K_{BA} & K_{BB} \end{bmatrix} \begin{bmatrix} \theta'_A \\ \theta'_B \end{bmatrix} \quad (17)$$

where  $K_{AA}$ ,  $K_{AB}$ ,  $K_{BA}$  and  $K_{BB}$  computed by Eqs. (18) to (21) are the components of the element stiffness matrix including moment and shear deformations.

$$K_{AA} = \frac{12 \prod_{i=1}^m EI_i}{L'_{Det}} (L'^2 GA_z f'_{BB} + 12 \prod_{i=1}^m EI_i) \quad (18)$$

$$-K_{AB} = -K_{BA} = \frac{12 \prod_{i=1}^m EI_i}{L'_{Det}} (L'^2 GA_z f'_{AB} - 12 \prod_{i=1}^m EI_i) \quad (19)$$

$$K_{BB} = \frac{12 \prod_{i=1}^m EI_i}{L'_{Det}} (L'^2 GA_z f'_{AA} + 12 \prod_{i=1}^m EI_i) \quad (20)$$

$$D_{et} = L'^2 GA_z (f'_{AA} f'_{BB} - f'_{AB}{}^2) + 12 \prod_{i=1}^m EI_i (f'_{AA} + f'_{BB} + 2f'_{AB}) \quad (21)$$

It is worth emphasizing, since the proposed equations in this section prepared a general formulation to figure out the stiffness matrix of each element with various flexibility throughout the length of it, the stiffness matrix of linear flexibility model can be derived adjusting the transformation points of LFM from end "A" and replacing into the mentioned relations.

### 2.2.2 Determination of the transformation points and flexibility of each part

As mentioned, in this study, the tangent stiffness matrix is obtained using one element for each member. To determine the transformation points and flexibility of each part, the assigned hysteric model (Fig. 4) (in this study, the vertex oriented is considered) is evaluated in the three points (ends "A" and "B" and middle point "C" shown in Fig. 5).

It should be noted, the moment of middle point (C) is calculated from statically equilibrium equation (without

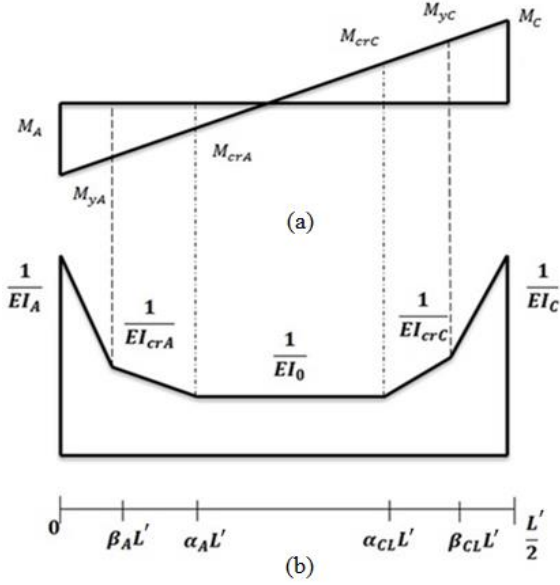


Fig. 6 The proposed plasticity model (a) the linear moment diagram (b) the flexibility distribution for the first half of beam element

subdividing member). For example, the bellow equation can be used to calculate the moment of point “C” when the uniform gravity load is applied

$$M_C = V_A \frac{L'}{2} + M_A - \frac{WL'^2}{8} \quad (22)$$

where  $M_C$  and  $M_A$  are the moments of points “C” and “A”, respectively.  $V_A$  is the shear of point “A” and “W” is uniform gravity load.

As it is evident in Fig. 4, the considered hysteric model is contained three states: (a) Loading (depicted “1”) (b) Unloading and reloading (depicted “2”) (c) Transition to vertex ((depicted “3”). Therefore, based on the state of points “A”, “B” and “C”, the transformation points and stiffness of each part are figured out. To do so, the moment diagram is assumed linear between “A” and “C” and also “C” and “B”. The circumstances for the first half of element (between “A” and “C”) is illustrated and the methodology will be same for the second half. The proposed model for the first half of beam is presented in Fig. 6.

As shown in Fig. 6, the cracked and the yielded lengths ( $\alpha L'$  and  $\beta L'$ ) are calculated based on linear moment diagram assumed between points “A” and “C”. The parameters  $\alpha$  and  $\beta$  are calculated from corresponding end as follows

$$\alpha_A = \frac{(M_{crA} - M_A)}{(M_C - M_A)} 0.5 \quad \text{for } |M_A| > |M_{crA}| \quad (23)$$

$$\beta_A = \frac{(M_{yA} - M_A)}{(M_C - M_A)} 0.5 \quad \text{for } |M_A| > |M_{yA}| \quad (24)$$

In the above equations,  $M_{crA}$ ,  $M_{crC}$  are the cracking moments in the ends “A” and “C”, respectively.  $M_{yA}$ ,  $M_{yC}$  are the yielding moments in the ends “A” and “C”, respectively. It is worth emphasizing that all coefficients ( $\alpha$  and  $\beta$ ) should be between 0 and 0.5.

Note: if  $M_A$  is positive, the values of  $M_y$  and  $M_{cr}$  for calculating  $\alpha$  and  $\beta$  will be positive (in Eqs. (23) and (24)) and vice versa. Coefficients  $\alpha$  and  $\beta$  for each end cannot be lower than the maximum of them ( $\alpha_{Max}$ ,  $\beta_{Max}$ ) in previous steps regardless the values of current moments. All calculated transformation points coefficients and corresponding stiffness are collected in collections “X” and “S”, respectively. The methodology to generate the collections “X” and “S” for end “A” is illustrated (for other points is the same):

a. If the state of end “A” is loading (in hysteric model):

In this state, two cases are considered for the moment diagram: single curvature and double curvature moment diagrams.

a-1 Single curvature  $M_A M_C > 0$

a-1-1  $|M_A| \leq |M_{crA}|$

$$\alpha_A = 0, \beta_A = 0$$

$$X_A = \{\beta_A, \alpha_A\}, S_A = \{EI_y, EI_{cr}\} \quad (25)$$

$EI_y$ ,  $EI_{cr}$  are the stiffness of yielding and cracking branches in hysteric model.

a-1-2  $|M_{crA}| < |M_A| \leq |M_{yA}|$

a-1-2-1  $|M_C| \leq |M_{crC}|$

$$\alpha_A = \frac{(M_{crA} - M_A)}{(M_C - M_A)} 0.5, \beta_A = 0$$

(26)

$$X_A = \{\beta_A, \alpha_A\}, S_A = \{EI_y, EI_{cr}\}$$

a-1-2-2  $|M_{crC}| < |M_C|$

$$\alpha_A = 0.25, \beta_A = 0$$

(27)

$$X_A = \{\beta_A, \alpha_A\}, S_A = \{EI_y, EI_{cr}\}$$

a-1-3  $|M_{yA}| < |M_A|$

a-1-3-1  $|M_{yC}| \geq |M_C|$

$$\alpha_A = \frac{(M_{crA} - M_A)}{(M_C - M_A)} 0.5, \beta_A = \frac{(M_{yA} - M_A)}{(M_C - M_A)} 0.5$$

(28)

$$X_A = \{\beta_A, \alpha_A\}, S_A = \{EI_y, EI_{cr}\}$$

a-1-3-2  $|M_{yC}| < |M_C|$

$$\alpha_A = 0, \beta_A = 0.25$$

(29)

$$X_A = \{\beta_A, \alpha_A\}, S_A = \{EI_y, EI_{cr}\}$$

a-2 Double curvature  $M_A M_C < 0$

In this case, the situations are completely similar to single curvature but in step a-1-2 and a-1-3,  $\alpha$  and  $\beta$  are obtained by Eqs. (26) and (28) regardless the value of “C” moment.

Note: In all steps, when  $\alpha_A$  or  $\beta_A$  is zero means that this transportation point and the corresponding stiffness ( $EI$ ) of it will be eliminated from collections “X” and “S”.

b. If the state of end “A” is unloading or reloading:

In this situation, the current line of moment diagram is compared with the previous one (the index of previous moment diagram is “P”) to determine the junction point ( $x_{junA}$ ) of two lines.

$$x_{junA} = \frac{1}{2} \frac{\Delta M_A}{\Delta M_A - \Delta M_C} (\Delta M_A = M_A - M_{AP}, \Delta M_C = M_C - M_{CP}) \quad (30)$$

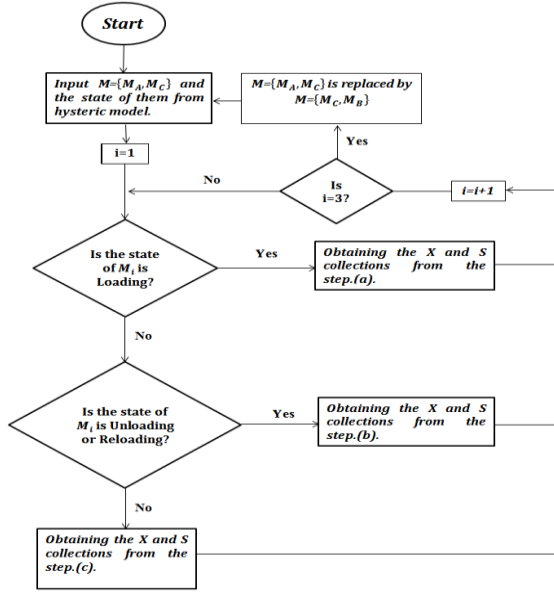


Fig. 7 The flowchart for determining the transformation points

The moment in junction point ( $M_{junA}$ ) will be

$$M_{junA} = 2(M_C - M_A)x_{junA} + M_A \quad (31)$$

$$\text{if } M_{junA}M_A \geq 0 \rightarrow \alpha_{UA} = \{x_{junA}\} \quad (32)$$

$$\text{if } M_{junA}M_A < 0 \rightarrow \alpha_{UA} = \{\min(x_{0A}, x_{0AP})\} \quad (33)$$

$$\text{where } x_{0A} = \frac{1}{2} \frac{(-M_A)}{(M_C - M_A)}, \quad x_{0AP} = \frac{1}{2} \frac{(-M_{Ap})}{(M_{Cp} - M_{Ap})}$$

After calculating  $\alpha_{UA}$ , the collections "X" and "S" are calculated as follows

b.1  $M_A \varphi_A < 0$

$$\text{b.1.1 } \alpha_{UA} \geq \alpha_{Amax} \rightarrow X_A = \{\alpha_{Amax}\}, S_A = \{EI_A\} \quad (34)$$

$$\text{b.1.2 } \alpha_{UA} < \alpha_{Amax} \rightarrow X_A = \{\alpha_{UA}, \alpha_{Amax}\}, S_A = \{EI_A, EI_{TA}\} \quad (35)$$

b.2  $M_A \varphi_A > 0$

$$\text{b.2.1 } \alpha_{UA} \geq \alpha_{Amax} \rightarrow X_A = \{\alpha_{Amax}\}, S_A = \{EI_A\} \quad (36)$$

$$\text{b.2.2 } \beta_{Amax} \leq \alpha_{UA} < \alpha_{Amax} \rightarrow X_A = \{\alpha_{UA}, \alpha_{Amax}\}, S_A = \{EI_A, EI_{crA}\} \quad (37)$$

$$\text{b.2.3 } \alpha_{UA} < \beta_{Amax} \rightarrow X_A = \{\alpha_{UA}, \beta_{Amax}, \alpha_{Amax}\}, S_A = \{EI_A, EI_{yA}, EI_{crA}\} \quad (38)$$

where  $EI_A$  means the current stiffness of end "A" based on hysteric model in unloading and reloading and  $EI_{TA}$  is the transition stiffness defined in step c.

c. If the state of end "A" is transition to vertex:

In this situation, collections "X" and "S" are

$$X_A = \{\alpha_{Amax}\}, S_A = \{EI_{TA}\} \quad (39)$$

$EI_{TA}$  is the current stiffness of point "A" in passing to vertex. It is worth mentioning, for end "C" in the first half and also points "C" and "B" in the second half, the a-c steps are same (index "A" in equations are substituted by "C" or "B"). The mentioned steps are summarized in Fig.

7.

Note: As manifested, in steps a-c, the transformation points coefficients are figured out from the corresponding end ("A", "C" and "B") regarded as an origin but in the final collection, all the coefficients  $\alpha$  and  $\beta$  (collection "X") should be calculated from end "A". So in the first half, the values of  $\alpha$  and  $\beta$  for end "C" will modify  $(0.5-\alpha)$  and  $(0.5-\beta)$ . In the second half the values for end "C" will change  $(0.5+\alpha)$  and  $(0.5+\beta)$ . The coefficients for end "B" will remold  $(1-\alpha)$  and  $(1-\beta)$ . After adjusting coefficients  $\alpha$  and  $\beta$ , collection "S" is rearranged according to altered coefficients  $\alpha$  and  $\beta$ .

Note: it should be emphasized that  $\alpha_A + \alpha_C$  (for the second half  $\alpha_C + \alpha_B$ ) should be lower than 0.5. When the whole of first half (or the second half) experienced inelastic deformation. The values of  $\alpha_A$  and  $\alpha_C$  (for the second half  $\alpha_C$  and  $\alpha_B$ ) should be altered to capture the actual flexibility. To do so, the junction point of the flexibility lines "a'" and the modified flexibility " $\frac{1}{EI'_0}$ " are calculated from Eqs. (40) and (41).

$$\alpha'_A = \frac{\frac{f_0 - f_{crA}}{\alpha_A - \beta_A} \beta_A + (f_0 - f_{crC}) \left( \frac{\beta_C}{\alpha_C} - 1 \right) + f_0 - f_{crA}}{\frac{f_0 - f_{crA}}{\alpha_A - \beta_A} + \frac{f_0 - f_{crC}}{\alpha_C}} \quad (40)$$

$$\frac{1}{EI'_0} = f'_0 = \frac{f_0 - f_{crA}}{\alpha_A - \beta_A} (\alpha'_A - \beta_A) L + f_{crA} \quad (41)$$

Where  $f'_0, f_0, f_{crA}, f_{crC}$  are the modified elastic flexibility, elastic flexibility, cracking flexibility of end "A" and cracking flexibility of end "C", respectively.

After doing the steps a-c for "A", "C" and "C", "B", the transformation points coefficients collection and the stiffness collection for the first and the second half is as follows

(a)  $\alpha_A + \alpha_C < 0.5$

$$X_{fh} = \{0, X_A, X_C, 0.5\} S_{fh} = \{S_A, EI_0, EI_0, S_C\} \quad (42)$$

(b)  $\alpha_A + \alpha_C = 0.5$

$$X_{fh} = \{0, X_A, X_C, 0.5\} S_{fh} = \{S_A, EI_0, S_C\} \quad (43)$$

And for the second half:

(a)  $\alpha_C + \alpha_B < 0.5$

$$X_{sh} = \{X_C, X_B, 1\} S_{sh} = \{S_C, EI_0, EI_0, S_B\} \quad (44)$$

(b)  $\alpha_C + \alpha_B = 0.5$

$$X_{sh} = \{X_C, X_B, 1\} S_{sh} = \{S_C, EI_0, S_B\} \quad (45)$$

In sum, the first and the second half will be assembled one to generate the final collection (Eq. (46))

$$X = \{X_{fh}, X_{sh}\}, S = \{S_{fh}, S_{sh}\} \quad (46)$$

The aforementioned methodology has some advantages:

- The stiffness matrix is obtained based on one element for each beam.

- The effect of gravity load is considered taking point "C" in middle length.

- The aforementioned methodology expands the plasticity along the length of member, although hysteric model is merely evaluated in three points.

- In this formulation, unlike some other spread plasticity models, yielded and cracked portions are separated.

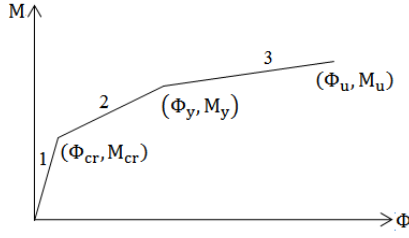


Fig. 8 Tri-linear moment curvature curve.

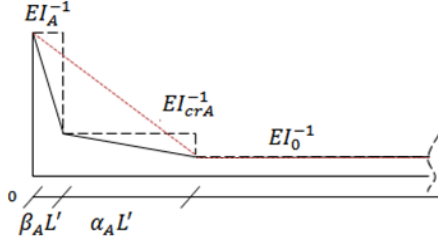


Fig. 9 Comparing the flexibility distribution of LFM and ILFM

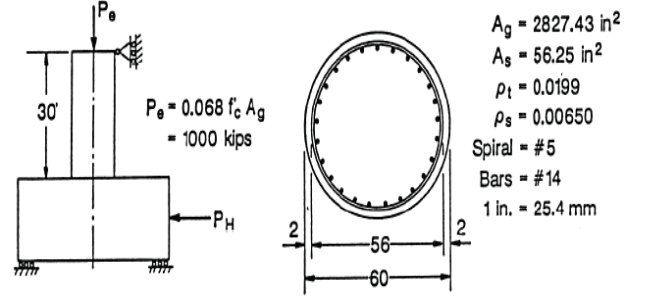
To explain the last advantage more, consider the three linear moment-curvature as depicted in Fig. 8, for a RC member. If the current moment of end “A” ( $M_A$ ) is more than the yielded moment ( $M_y$ ), the changes of flexibility for end “A” in LFM and ILFM will be according to what is demonstrated in Fig. 9.

In Fig. 9, the actual flexibility distribution (dashed black lines) is compared with LFM (dotted red lines) and ILFM (black lines). As it is clear, although both LFM and ILFM take the flexibility distribution into consideration with approximation, the ILFM presents more compatible flexibility distribution with precise one.

The methodology for column members is similar to beam elements. For these members, the hysteric model is only evaluated in two ends of element because of the absence of perpendicular gravity load to the axis of them.

### 2.2.3 Modifying the effects of applied gravity load on end moments and shears

When structural elements encounter non-uniform stiffness, the effects of applied gravity load on end moments and shears should be altered. To figure out these effects for a member that is subdivided by “m” transformation points, the least work method is utilized in this study. In this section, to derive the simple and practical formulations, the stiffness of each part (between two successive transformation points) is considered uniform and equal to the average of two successive stiffness (for example, the stiffness of the part between (i)<sup>th</sup> and (i+1)<sup>th</sup> transformation points is  $\frac{EI_i + EI_{i+1}}{2}$ ). In the least work method, first the internal strain energy is obtained. After that, the first partial derivative of the mentioned energy with respect to the applied force (here left end moment ( $M_A$ ) and shear force ( $V_A$ ) of end “A” according to Fig. 4) is equal to deflection here zero at the point of considered force (Eqs. (47)-(48)). Finally, these equations are simultaneously solved to gain the  $M_A$  and  $V_A$ . The outcomes are expressed in the Eqs. (49)-(50).


 Fig. 10 Configuration of full scale bridge (Reinhorn *et al.* 2009)

$$\frac{\partial U}{\partial M_A} = M_A P_1 + V_A P_2 - \frac{W}{2} P_3 = 0 \quad (47)$$

$$\frac{\partial U}{\partial V_A} = M_A P_2 + V_A P_3 + \frac{V_A L'}{GA_z} - \frac{W}{2} P_4 - \frac{wL'^2}{2GA_z} = 0 \quad (48)$$

$$V_A = \frac{WP_3 - 2M_A P_1}{2P_2} \quad (49)$$

$$M_A = \frac{WGA_z P_2 P_4 - P_2 WL'^2 - GA_z WP_3 (P_3 + \frac{L'}{GA_z})}{2GA_z (P_2^2 - P_1 (P_3 + \frac{L'}{GA_z}))} \quad (50)$$

Where

$$P_1 = L' \left( \sum_{i=1}^{m-1} \left( \frac{1}{EI_i} - \frac{1}{EI_{i+1}} \right) \times x_i^1 \right) + \frac{1}{EI_m} x_m^1 \quad (51)$$

$$P_2 = \frac{L'^2}{2} \left( \sum_{i=1}^{m-1} \left( \frac{1}{EI_i} - \frac{1}{EI_{i+1}} \right) \times x_i^2 \right) + \frac{1}{EI_m} x_m^2 \quad (52)$$

$$P_3 = \frac{L'^3}{3} \left( \sum_{i=1}^{m-1} \left( \frac{1}{EI_i} - \frac{1}{EI_{i+1}} \right) \times x_i^3 \right) + \frac{1}{EI_m} x_m^3 \quad (53)$$

$$P_4 = \frac{L'^4}{4} \left( \sum_{i=1}^{m-1} \left( \frac{1}{EI_i} - \frac{1}{EI_{i+1}} \right) \times x_i^4 \right) + \frac{1}{EI_m} x_m^4 \quad (54)$$

In Eqs. (47)-(48),  $U$  is the internal strain energy. After computing the  $M_A$  and  $V_A$ ,  $M_B$  and  $V_B$  are figured out using the statically equilibrium equations

$$V_B = WL - V_A \quad (55)$$

$$M_B = V_A \times L + M_A - \frac{WL^2}{2} \quad (56)$$

It should be pointed out that in the present study, Eqs. (47)-(56) are extracted for beam elements merely subjected to uniform gravity load that is the most probable kind of gravity loads in the building frames but the aforementioned equations can be altered and extended using explained method to any arbitrary gravity loads.

### 3. Nonlinear analysis

The actual behavior of a building frame can be varied between fully elastic and collapse. The moment-curvature relation of every RC structural element has a definitive

effect on the behavior of structure. In this research, the tri-linear moment-curvature relation, as shown in Fig. 8, is used for expressing the nonlinear behavior of reinforced concrete sections.

The moment-curvature characters are computed based on limitations and relations presented in (Park and Paulay 1975, Park and Ang 1985).

In present study, the effect of rigid length zone is considered to simulate the increase of stiffness in joints using following transformations (Habibi and Moharrami 2010)

$$\begin{aligned} \begin{bmatrix} M_A \\ M_B \end{bmatrix} &= [\tilde{L}] \begin{bmatrix} M'_A \\ M'_B \end{bmatrix}, \quad \begin{bmatrix} \theta'_A \\ \theta'_B \end{bmatrix} = [\tilde{L}]^t \begin{bmatrix} \theta_A \\ \theta_B \end{bmatrix}; \\ [\tilde{L}] &= \frac{1}{1 - \lambda_A - \lambda_B} \begin{bmatrix} 1 - \lambda_B & \lambda_A \\ \lambda_B & 1 - \lambda_A \end{bmatrix} \end{aligned} \quad (57)$$

where  $\lambda_A$  and  $\lambda_B$  are the proportions of rigid zone at the element ends. Taking all the forces perpendicular to the axis of the element into account, the element stiffness matrix relating displacements and forces, is obtained as follows (Habibi and Moharrami 2010)

$$K = R_E K_S R_E^T \quad (58)$$

where

$$R_E^T = \begin{bmatrix} -\frac{1}{L} & 1 & \frac{1}{L} & 0 \\ -\frac{1}{L} & 0 & \frac{1}{L} & 1 \end{bmatrix}; \quad K_S = \tilde{L} K'_S \tilde{L}^{-1} \quad (59)$$

The axial and geometric stiffness matrices are added to element stiffness matrix as it is considered by Habibi and Moharrami (Habibi and Moharrami 2010).

In present research, it is assumed that the effects of applied gravity loads are altered in each step of incremental nonlinear analysis because of changing the flexibility properties of members along the analysis; therefore, the gravity load effects are updated on the structural elements in each step of analysis and lateral loads are algebraically added to it. The Newton-Raphson method is applied to nonlinear analysis of structures.

## 4. Numerical examples

### 4.1 Example 1

The first example is a circular column that has been tested at the laboratories of the National Institute of Standards and Technology (Stone and Cheok 1989). This column represents typical bridge pier designed in accordance with Caltrans specifications (Caltrans 1988). The column is tested by applying both axial and lateral loads. The characters of this column are depicted in Fig. 10. The concrete has a compressive strength of 35.85 MPa (5.2 ksi) and a modulus of elasticity of 28.34 GPa (4110 ksi). The steel used for longitudinal reinforcement has a yield strength of 475.05 MPa (68.9 ksi) and modulus of elasticity of 189.18 GPa (27,438 ksi). The axial load applied to the specimen is 4450 kN (1000 kips). More details have been presented by Reinhorn *et al.* (2009).

The vertex-oriented hysteric model is considered for the

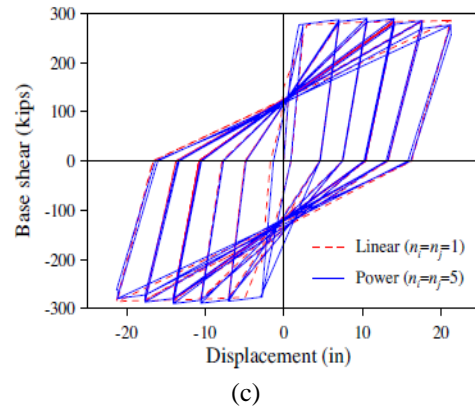
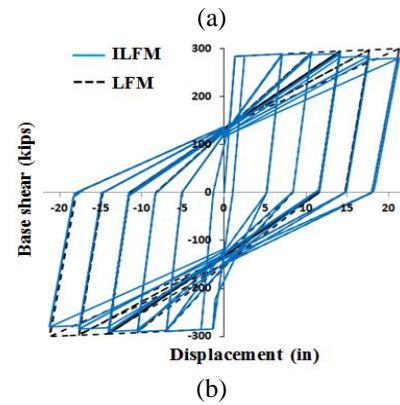
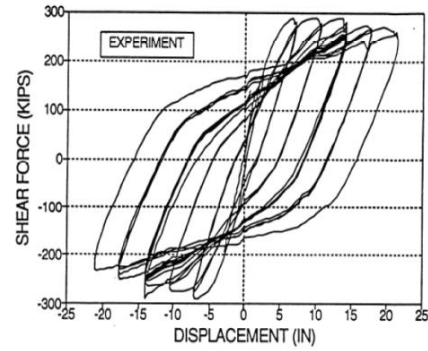


Fig. 11 The pier outcomes (a) experimental (Reinhorn *et al.* 2009) (b) improved and linear spread plasticity model with moderate stiffness and strength degradation (c) Power and linear plasticity model (Roh *et al.* 2012)

column and this pier is tested using the displacement control quasi-static loading history. The experimental outcomes are shown in Fig. 11(a). This column is analyzed applying the proposed spread plasticity model in this study and results are compared with the linear plasticity model of IDARC in Fig. 11(b). It is worth pointing out that the mentioned pier has been also evaluated by Roh *et al.* (2012) using power spread plasticity model. The outcomes of power and linear plasticity model have been compared by Roh *et al.* (2012), as shown in Fig. 11(c).

As it is clear in Fig. 11, the result of ILFM has good agreement with experimental outcomes. The consequence for Power Spread Plasticity Model (PSPM) (Fig. 11(c)) is analogous. It seems, by increasing displacement, the gap between ILFM as well as PSPM and LFM will be higher. The strength reductions in ILFM and PSPM rather than

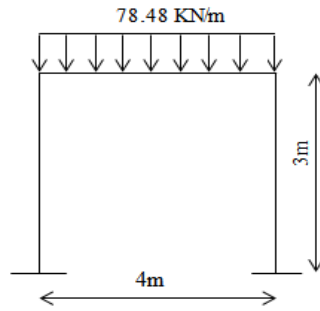


Fig. 12 One-story RC frame (Habibi 2007)

Table 1 Cross-sectional characteristics of beam and columns

Element type	Dimension (mm)		Reinforcement (mm <sup>2</sup> )	
	Width	Height	Bottom	Top
Beam	254	635	2040	1020
Both columns	254	635	2040	2040

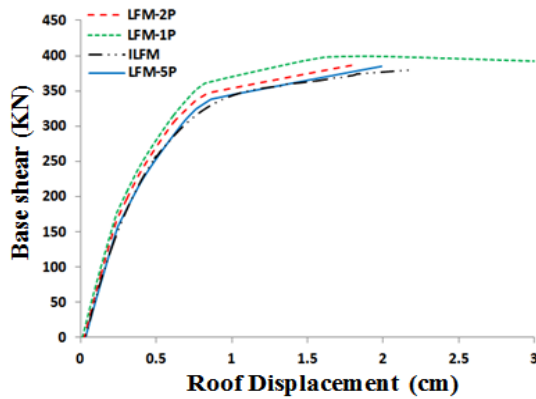


Fig. 13 Comparing the results of ILFM with LFM-1P, LFM-2P and LFM-5P

LFM are estimated more compatible with experimental results. It should be noted, although for column element, there are not distributed perpendicular forces along the member; not separating the yielded and cracked lengths causes some errors in LFM analysis. In the ILFM, these lengths have been separated completely. The power spread plasticity model almost has obviated this problem too; therefore, as depicted in Fig. 9, the outcomes of ILFM and PSPM have good agreement.

#### 4.2 Example 2

The second example is an one-story, one-bye planner moment resistant reinforced concrete frame as described in Fig. 12 (Habibi 2007). The concrete is assumed to have a cylinder strength of 20.7 Mpa, a modulus of rupture of 2.83 Mpa, a modulus of elasticity of 22070 Mpa, a strain of 0.002 at maximum strength and an ultimate strain of 0.004. The steel has a yield strength of 276 Mpa and a modulus of elasticity of 200,000 Mpa. A uniformly distributed gravity load of 78.48 kN/m is applied on the beam. Reinforcements have the cover to the steel centroid of 51 mm. It is assumed

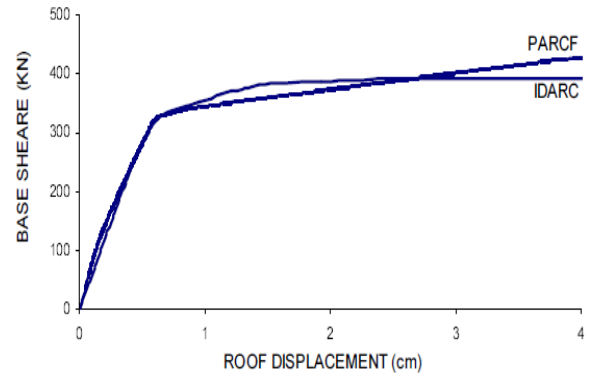


Fig. 14 Results of previous analyzes on one-story, one-bye frame (Habibi 2007)

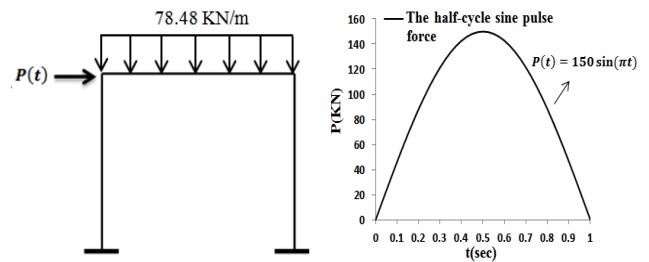


Fig. 15 The one-story, one-bye frame and imposed loads

that columns and beams have rectangular cross sections detailed in Table 1. Two analyses are carried out on this frame separately. First, the pushover analysis is done on the frame to assess the proposed methodology from elastic to collapse. This analysis is carried out on this frame using ILFM and increasing lateral loads considering power distribution from FEMA273 (1997) along with constant gravity loads. Then linear flexibility model in IDARC2D (Reinhorn *et al.* 2009) is utilized to accomplish pushover analysis on the mentioned frame. Analyses in IDARC2D are performed several times by considering the different number of beam elements taken one, two and five (named afterward LFM-1P, LFM-2P and LFM-5P, respectively). The outcomes are described in Fig. 13. The capacity curve of the structure has been achieved by applying the LFM by Habibi (2007), as shown in Fig. 14.

As shown in Fig. 13, the gap between the results of ILFM and LFM-1P is not negligible. It seems, the significant gravity load in this example is the main reason for the mentioned gap. The difference between LFM-2P and LFM-5P with ILFM is low because, as mentioned (for linear flexibility model), in the cases of significant gravity load, structural elements should be subdivided to capture this effect (Reinhorn *et al.* 2009). Comparing the LFM results with those of ILFM exhibits that by increasing number of elements from 1 to 5 results of LFM converge to ILFM results. This matter verifies the ILFM results. Contrasting the outcomes of LFM-1P (Fig. 13) and IDARC (Fig. 14) confirms the modeling of the frame in this study.

The nonlinear dynamic analysis is also performed on the frame subjected to the half-cycle sine pulse force presented in Fig. 15. To evaluate the accuracy of the suggested model, the nonlinear analysis is accomplished once using ILFM and again with SeismoStruct (2016). In SeismoStruct, to

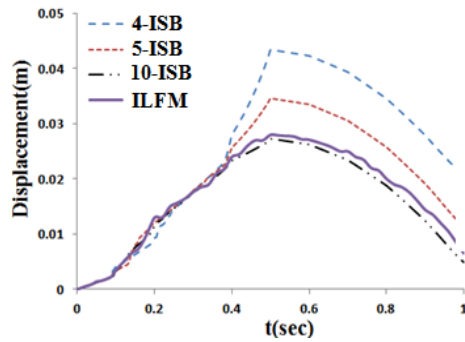


Fig. 16 Comparing the results of ILFM with 4-ISB, 5-ISB and 10-ISB

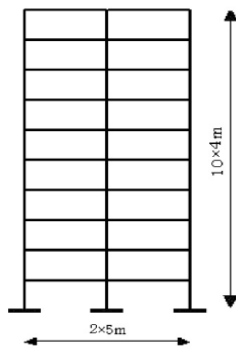


Fig. 17 Ten-story RC frame (Habibi and Moharrami 2010)

model structural elements, the inelastic force-based frame element type-infrmFB is applied. This model is the most accurate among the four frame element types of SeismoStruct, since it is capable of capturing the inelastic behavior along the entire length of a structural member, even when employing a single element per member (SeismoStruct 2016), is used to model the beam and columns. The number of element's integration sections is considered four, five and ten (named afterward 4-ISB, 5-ISB and 10-ISB). The number of used section fibers in equilibrium computations carried out at each of the element's integration sections is taken 150 fibers into account. The Lobatto quadrature is employed for the considered integration sections. The outcomes of analyzes are shown in Fig. 16.

Comparing consequences describes the number of element's integration sections has glaring effect on results. By increasing the number of element's integration sections, the plasticity distribution along the member will be modeled closer to actual behavior of structure. As exhibited in Fig. 16, the outcomes of ILFM and SeismoStruct (2016) with ten element's integration sections are compatible. The peak of roof displacement is 4.3 cm and 2.7 cm for 4-ISB and 10-ISB, respectively. The roof displacement is dwindled increasing the number of element's integration sections. The gap between the curve of 4-ISB and 10-ISB demonstrates the effect of selecting element's integration sections on results. Contrasting the ILFM and 10-ISB clarifies acceptable approximation of the proposed methodology.

### 4.3 Example 3

The last example is a ten-story, two-bay planner moment

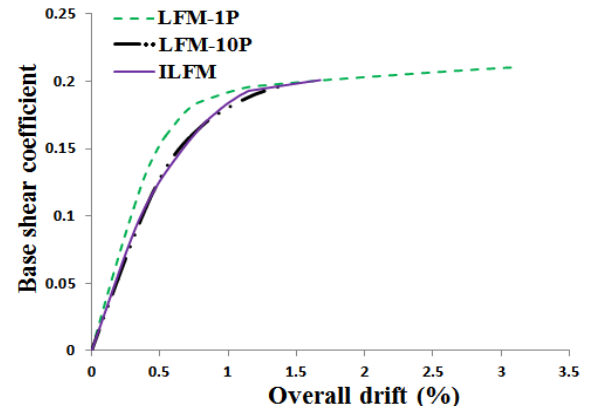


Fig. 18 The results of ILFM with LFM-1P and LFM-10P

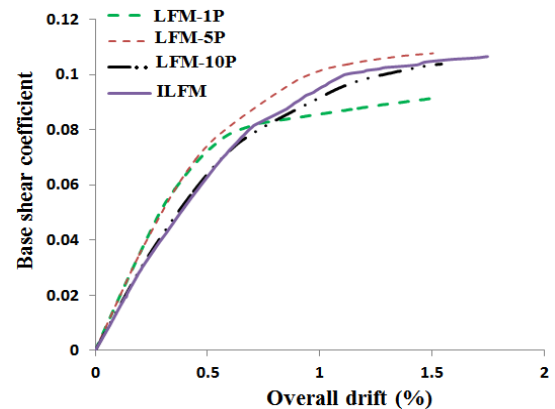


Fig. 19 The outcomes of ILFM with LFM-1P, LFM-5P and LFM-10P

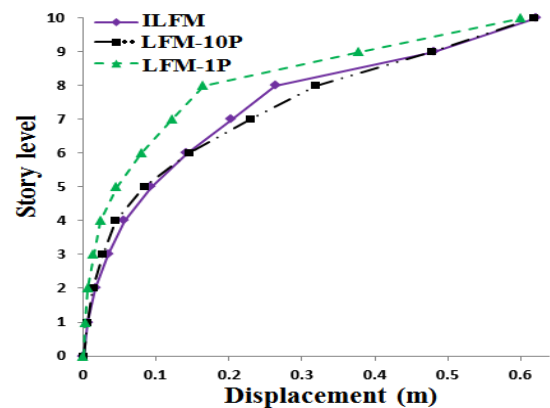


Fig. 20 The story displacements of ILFM with LFM-1P and LFM-10P in overall drift 1.5%

resistant reinforced concrete frame shown in Fig. 17 (Habibi and Moharrami 2010). The concrete is assumed to have a cylinder strength of 30 MPa, a modulus of rupture of 3.45 MPa, a modulus of elasticity of 27,400 MPa, a strain of 0.002 at maximum strength and an ultimate strain of 0.004. The steel has a yield strength of 300 MPa and a modulus of elasticity of 200,000 MPa.

Pushover analysis is performed on this frame two times with different gravity loads. In the former, a uniformly distributed gravity load applied on all beams is 20 kN/m. To analyze this example, ILFM and LFM are utilized. In the linear flexibility, once each member considered one (LFM-

1P) and then each member is subdivided ten elements (LFM-10P). The results of these analyzes are depicted in Fig. 18.

Contrasting the outcomes of ILFM and LFM-10P shows that these models are great compatible. The maximum overall drift for ILFM is almost 1.8% and for LFM-10P is about 1.3%. Although there is a difference between the results of LFM-1P and ILFM for overall drift 0.4 to 1 percent, in other ranges, consequences are close to each other. It seems, for the mentioned gravity loads, the effect of lateral load is dominated.

In the latter, the distributed gravity load imposed on beams is considered 35 KN/m to assess the presented model for significant gravity loads. In this case too, linear flexibility model is used to analyze several times. In the first one, each element considered one. In the second and third analyze, elements are subdivided five and ten parts (LFM-5P and LFM-10P). After the aforementioned analyses, the present formulation is utilized to perform pushover analysis. The results of these analyses are indicated in Fig. 19. The floor displacements for overall drift 1.5 percent are displayed in Fig. 20.

As shown in Fig. 19, applying more subdivided part for each element decreases the differences between the results of linear flexibility model and ILFM. Comparing the consequences of LFM-1P and ILFM illustrates that the gap between two curves increases with augmentation of inelastic deformation. The result of LFM-5P is closer to ILFM rather than LFM-1P. The LFM-10P has the most compatibility with ILFM between all models. As demonstrated in Fig. 20, the result of LFM-1P has noticeable difference with ILFM and LFM-10P. This contrast refers to the shortcomings of this model in taking gravity load effect into account.

## 5. Conclusions

In this study, the linear flexibility model is improved for taking both the effects of lateral and gravity loads into account. Against to other spread plasticity models, in the proposed model, there is no need to subdivide members into several elements for considering the gravity load effects. Using merely one element for each member can dwindle computational time of analysis. Three examples from previous studies are selected to evaluate the accuracy of the suggested model. Comparing the results of the proposed model with experimental, the linear flexibility and power plasticity models confirms the accuracy of the improved model. It is demonstrated that linear flexibility model considering the member as one element produces cumulative errors and leads to incorrect results. It is described that proposed plasticity model can simultaneously account for gravity and lateral load effects by using only one element for each reinforced concrete member without subdividing the member. By comparing the LFM and ILFM outcomes, it is observed that by increasing the number of elements, the consequences of the linear flexibility model converge to proposed flexibility model. The outcomes illustrate an increase gap between ILFM and LFM when the gravity load is developed.

## References

- Al-Haddad, M.S. and Wight, J.S. (1988), "Relocating beam plastic hinging zones for earthquake resistant design of reinforced concrete buildings", *ACI Struct. J.*, **85**(2), 123-133.
- Alva, G.M.S. and De Cresce El, A.L.H. (2010), "Application of lumped dissipation model in nonlinear analysis of reinforced concrete structures", *Eng. Struct.*, **32**(4), 974-981.
- Anderson, J.C. and Townsend, W.H. (1977), "Models for RC frames with degrading stiffness", *J. Struct. Div.*, **103**(12), 2361-2376.
- Aoyama, H. and Sugano, T. (1968), *A Generalized Inelastic Analysis of Reinforced Concrete Structures Based on the Tests of Members*, Recent Researches of Structural Mechanics, Contributions in Honor of the 60<sup>th</sup> Birthday of Prof. Y. Tsuboi, Uno Shoten, Tokyo, Japan, 15-30.
- Birely, A.C., Lowes, L.N. and Lehman, D.E. (2012), "A model for the practical nonlinear analysis of reinforced-concrete frames including joint flexibility", *Eng. Struct.*, **34**, 455-465.
- Caltrans (1988), *Bridge Design Specifications*, California Department of Transportation, Division of Structures, Sacramento, U.S.A.
- Clough, R.W. (1966), "Effect of stiffness degradation on earthquake ductility requirements", Ph.D. Dissertation, University of California, U.S.A.
- FEMA273 (1997), *NEHRP Guideline for the Seismic Rehabilitation of Buildings*, Federal Emergency Management Agency, Washington, U.S.A.
- Giberson, M.F. (1967), *The Response of Nonlinear Multi-Story Structures Subjected to Earthquake Excitation*, California Institute of Technology.
- Habibi, A. and Moharrami, H. (2010), "Nonlinear sensitivity analysis of reinforced concrete frames", *Fin. Elem. Anal. Des.*, **46**(7), 571-584.
- Habibi, A.R. (2007), "Optimal seismic performance-based design of 2D RC frameworks", Ph.D. Dissertation, Tarbiat Modares University, Tehran, Iran.
- Hajjar, J.F., Molodan, A. and Schiller, P.H. (1998), "A distributed plasticity model for cyclic analysis of concrete-filled steel tube beam-columns and composite frames", *Eng. Struct.*, **20**(4), 398-412.
- Inel, M. and Ozmen, H.B. (2006), "Effects of plastic hinge properties in nonlinear analysis of reinforced concrete buildings", *Eng. Struct.*, **28**(11), 1494-1502.
- Iu, C.K. (2016), "Nonlinear analysis of the RC structure by higher-order element with the refined plastic hinge", *Comput. Concrete*, **17**(5), 579-596.
- Izadpanah, M. and Habibi, A. (2015), "Evaluating the spread plasticity model of IDARC for inelastic analysis of reinforced concrete frames", *Struct. Eng. Mech.*, **56**(2), 169-188.
- Kim, S.P. and Kurama, Y.C. (2008), "An alternative pushover analysis procedure to estimate seismic displacement demands", *Eng. Struct.*, **30**(12), 3793-3807.
- King, W., White, D. and Chen, W. (1992), "Second-order inelastic analysis methods for steel-frame design", *J. Struct. Eng.*, **118**(2), 408-428.
- Kunnath, S.K. and Reinhorn, A.M. (1989), *Inelastic Three-Dimensional Response Analysis of Reinforced Concrete Building Structures (IDARC-3D)*, National Center for Earthquake Engineering Research, State University of New York at Buffalo, U.S.A.
- Lee, C.L. and Filippou, F.C. (2009), "Efficient beam-column element with variable inelastic end zones", *J. Struct. Eng.*, **135**(11), 1310-1319.
- Mander, J.B. (1984), "Seismic design of bridge piers", Ph.D. Dissertation, University of Canterbury, New Zealand.
- McGuire, W. (1993), *Plastic Hinge Based Methods for Advanced*

- Analysis and Design of Steel Frames: An Assessment of the State-of-the-Art*, Structural Stability Research Council, Bethlehem, Elsevier.
- Nguyen, P.C. and Kim, S.E. (2014), "Distributed plasticity approach for time-history analysis of steel frames including nonlinear connections", *J. Constr. Steel Res.*, **100**, 36-49.
- Otani, S. and Sozen, M.A. (1972), *Behavior of Multistory Reinforced Concrete Frames During Earthquakes*, University of Illinois Engineering Experiment Station, College of Engineering, University of Illinois at Urbana-Champaign, U.S.A.
- Park, R. and Paulay, T. (1975), *Reinforced Concrete Structures*, John Wiley & Sons.
- Park, Y.J. and Ang, A.H.S. (1985), "Mechanistic seismic damage model for reinforced concrete", *J. Struct. Eng.*, **111**(4), 722-739.
- Park, Y.J., Reinhorn, A.M. and Kunnath, S.K. (1987), *IDARC: Inelastic Damage Analysis of Reinforced Concrete Frame-Shear-Wall Structures*.
- Reinhorn, A.M., Roh, H., Sivaselvan, M., Kunnath, S.K., Valles, R.E., Madan, A., Li, C., Lobo, R. and Park, Y.J. (2009), *IDARC 2D Version 7.0: A Program for the Inelastic Damage Analysis of Structures*, MCEER Technical Report-MCEER-09-0006, University at Buffalo-the State University of New York, U.S.A.
- Roh, H., Reinhorn, A.M. and Lee, J.S. (2012), "Power spread plasticity model for inelastic analysis of reinforced concrete structures", *Eng. Struct.*, **39**, 148-161.
- SeismoStruct (2016), *A Computer Program for Static and Dynamic Nonlinear Analysis of Framed Structures*.
- Stone, W.C. and Cheok, G.C. (1989), *Inelastic Behavior of Full-Scale Bridge Columns Subjected to Cyclic Loading*, NIST Building Science Series 166, National Institute of Standards and Technology, Gaithersburg, U.S.A.
- Takizawa, H. (1973), "Strong motion response analysis of reinforced concrete buildings", *Concrete J.*, **11**(2), 10-21.
- White, D.W. (1993), "Plastic-hinge methods for advanced analysis of steel frames", *J. Constr. Steel Res.*, **24**(2), 121-152.
- Zhao, X.M., Wu, Y.F. and Leung, A. (2012), "Analyses of plastic hinge regions in reinforced concrete beams under monotonic loading", *Eng. Struct.*, **34**, 466-482.